isvr Institute of Sound and Vibration Research

Preliminary Considerations on Principles for the Determination of Difficult Bubble Parameters in situ through Megafrexel High Speed Photographic Observation

T.G. Leighton

ISVR Technical Report No 321

December 2007

University of Southampton

SCIENTIFIC PUBLICATIONS BY THE ISVR

Technical Reports are published to promote timely dissemination of research results by ISVR personnel. This medium permits more detailed presentation than is usually acceptable for scientific journals. Responsibility for both the content and any opinions expressed rests entirely with the author(s).

Technical Memoranda are produced to enable the early or preliminary release of information by ISVR personnel where such release is deemed to the appropriate. Information contained in these memoranda may be incomplete, or form part of a continuing programme; this should be borne in mind when using or quoting from these documents.

Contract Reports are produced to record the results of scientific work carried out for sponsors, under contract. The ISVR treats these reports as confidential to sponsors and does not make them available for general circulation. Individual sponsors may, however, authorize subsequent release of the material.

Preliminary Considerations on Principles for the Determination of Difficult Bubble Parameters *in situ* Through Megafrexel High Speed Photographic Observation

T G Leighton

ISVR Technical Report No. 321

December 2007

UNIVERSITY OF SOUTHAMPTON

INSTITUTE OF SOUND AND VIBRATION RESEARCH

FLUID DYNAMICS AND ACOUSTICS GROUP

Preliminary Considerations on Principles for the Determination of Difficult Bubble Parameters *in situ* Through Megafrexel High Speed Photographic Observation

by

T G Leighton

ISVR Technical Report No. 321

December 2007

Authorized for issue by
Professor R J Astley, Group Chairman

ACKNOWLEDGEMENTS

This work is funded by the Engineering and Physical Sciences Research Council, Grant number EP/D000580/1 (Principal Investigator: TG Leighton). The author is very grateful to Paul White, Zygmunt Klusec and Agni Mantouka for valuable discussions.

CONTENTS

ABSTRACT

An increasing number of laboratories have the facilities to take high speed photographs of the pulsations of microbubbles to a degree not previously possible. Together with the advent of ultrasonic contrast agents which are stable over a long period, and the use of techniques to locate them within the field of view, these experimental utilities enable movies to be made of the pulsation of bubbles with much finer spatial and temporal scales. The quantitative analysis of such movies, if it occurs, relies on fitting with models that contain several unknowns. This paper discusses in a preliminary manner how such movies can be interpreted in a way which reduces the reliance on uncertain fits of models to data, given that the movie provides basic dynamic information in the form of a time step and a bubble size and shape. If the driving acoustic field, including its phase with respect to the movie frames, is recorded, then the movie data can be interpreted directly in terms of key bubble parameters without fitting.

LIST OF FIGURES

Figure **Page**

1 Introduction

In some respects, the ever-increasing computing power that is becoming available can make models less useful. Whilst enhanced computational facilities undoubtedly bring benefits, they also bring disadvantages in that ingenious methods common to experimentalists a century ago may be neglected in favour of easier routes. As models increase in complexity, it can become a far more attractive proposition to code up equations quoted directly from other authors (or even to adopt the codes programmed from another user) than it is to re-derive the equations. This approach sidesteps an important process, since such re-derivation would provide the programmer with an appreciation of the model's underlying assumptions and inherent limitations, and therefore the degree to which the model is appropriate to the situations to which it is being applied. Furthermore, if such models are used to determine unknown parameters through fitting or inversion, the sophistication of the model and the result of a best fit may hide the fact that, if one of the fixed input values is erroneous, or if the physics inherent in the model does not reflect the environment with sufficient accuracy, then the result of the fit may be wrong. This is because the best-fit or inversion can be adjusting the value of the unknown parameter in a way which attempts to account for the erroneous value of the fixed input, or erroneous physics in the model [1]. There is a wealth of examples of this from the field of bubble acoustics. For example, if acoustic attenuation in the frequency range $f_{\min}$ to $f_{\max}$ is inverted to obtain the bubble size distribution, but the characteristics of that inversion erroneously assumes there exist no bubbles with resonances less than $f_{\min}$ or greater than $f_{\max}$, then the estimated bubble numbers may be erroneously augmented to account for any attenuation caused by bubbles with resonances less than $f_{\min}$ or greater than $f_{\max}$. Similarly, if the volume velocity $\dot{V}$ of a bubble is assumed to equal $4\pi R_0^2 \dot{R}$ instead of $4\pi R^2 \dot{R}$, then the assumption has been made that the radiating bubble acts as a rigid pulsator [2]. As a result, not only is the contribution of the oscillating gas pressure to the radiation neglected, but higher order terms (which may be necessary in later expansions) have already been neglected.

Therefore although increasing computing power makes it more feasible to invert models of increasing complexity, and indeed frequently offers a cheaper and quicker route to providing an answer than analytical or experimental approaches, there are complementary options to such 'blind' inversion. The one studied here is found in the employment of a more critical assessment of the relationship between the model and the experimental observable. Such assessment might provide a more accurate answer, or at least provide an indication of the extent to which the given answer might be inaccurate. This complementary approach should be a particularly important element in student training.

This report provides two examples of how such considerations may be applied in bubble acoustics, specifically: determination of the stiffness and dissipation of a pulsating bubble; and determination of the 'true' value of the surface tension of a gas bubble. These two examples were chosen because of the possibilities for observation which are opening up through the increasing access to high speed cameras (which are producing superb results [3-7]), coupled with the availability of controlled bubbles in the form of biomedical ultrasonic contrast agents which, although able to provide a controlled population, nevertheless require techniques which can provide estimates of key dynamic parameters associated with the gas, the wall, and the fluxes across it.

Just as increased computing power has opened up opportunities for use of sophisticated modelling, fitting and inversion, so have advances in data acquisition provided remarkable facilities for making direct observations of bubbles to support the approaches of this paper. Today high speed imaging at >10 million frames per second (fps) is accessible, and cameras capable of 10^6 fps are available for hire by most laboratories in the developed world, with sufficient light sensitivity to image fields of view of micrometre order. Furthermore, unless specific measures were taken (such as using acoustic or optical radiation forces, or confining the bubbles in a vessel, which can in principle affect bubble stability; [8-11]), past photographic investigations could be confounded by the low odds of finding a microbubble within the field of view. Now there are now common methods for placing and holding long-lived bubbles (in the form of ultrasonic contrast agents) within that field of view [12]. This then opens up the possibility of, for example, viewing the vessel walls not as a method of *in vitro* confinement which regrettably violates the assumption of a bubble

in an infinite free field inherent in the theory to which the observation is compared (as was the case in the past), but rather of studying the effect on the bubble dynamics of the vessel walls themselves, since *in vivo* the bubbles of interest may well be similarly confined [13-22].

Therefore the facilities for photographing the stable pulsations of microbubbles are significantly greater and more widespread than they were in the past. In the early 1990s, when megafrexel (10^6 fps) framing rates were available only to very few laboratories [23-26], and whilst in other laboratories flash photography provided some spectacular single images, extraordinary conditions had to be contrived to provide movies of individual bubbles undergoing pulsation and shape oscillation [27,28], or collapse, jetting and fragmentation [24,29-33]. Today, such events can be filmed under standard *in vitro* conditions [34]. Similarly the acquisition of 200 s of data for events of 10 ns duration took extraordinary measures [35,36] whilst today the real-time acquisition of >GB of data is available. For example, today even an inexpensive PC can achieve high data transfer rates (e.g. 320 MB/s for a SCSI interface, 375 MB/s for a SATA 300 interface).

2 Bubble dynamics in *PVt* Space: visualisation of the stiffness and dissipation

The ubiquitous method of representing bubble pulsation, through modelling or measurement (using high speed imaging (see section 1), or the scattering of light [37-39] or ultrasound [40] etc.), is by plotting the time history of the bubble radius R or volume V. However the passage of time t can also be tracked through the driving pressure, as it evolves in time, and therefore it is possible to envisage the volume time history of as a projection onto 2D space of a 3D plot of the driving pressure, the bubble volume, and the time. However the 2D projection of this onto PV space allows the flow of energy to be appreciated [28-44]. This is shown schematically on Figure 1(a) for (i) the stiffness-controlled regime, (ii) resonance, and (iii) the inertia-controlled regime. As time progresses a locus of points is mapped out by the pulsation

in *PV* space, and the area enclosed by each loop represents the $\int P\mathrm{d}V$ energy transfer, the direction of which following readily from the clockwise or counter-clockwise direction by which the loop is mapped out as *t* increases, allowing for example one to distinguish between multi-loop oscillations where the flow of energy is into the bubble during one loop and out of the bubble in the other, from those where the flow of energy is the same direction for both loops. Similarly, experimentally measured volume time histories can therefore be represented in this way and used to visualise energy flow. Net losses can be calculated by a $\int P\mathrm{d}V$ integration[1], and if the loops do not replicate exactly in each cycle, integration of the area over many loops on the steady state, and division by the number *N* of loops, reduces the end-error in the start and end of the integration by a factor of *N*.

Consider the pulsation shown in Figure 4.35 of reference [45]. Plots of the time history of volume from such a figure could be used to show which of several models (differing most noticeably by their damping) best predicts the measured oscillation. However before assessing the effect of changes to the dissipation in this way, it is best first to determine the stiffness, as opposed to obtain it from a fit.

Assume therefore that a record of bubble size time history is made (through high speed photography (section 1), Mie scattering [37-39], or envelope modulation of a high frequency ultrasonic beam [40] etc.) when it is driven by an applied pressure field *P(t)* which is uniform over the bubble wall at any instant (assume that all the wavenumbers *k* associated with *P(t)* obey $kR_0 \langle\langle 1$). It is important that the phase of the *applied* field be recorded in synchrony with the bubble motion. This will require experimental practicalities such as keeping far enough from the bubble so that the radiated field does not dominate the hydrophone emission, but not so far that a significant phase difference is introduced: presumably a record is made in the absence of the bubble, and then synchronised to the hydrophone record made in the presence of the bubble. As a result, whilst the bubble pulsates under a driving sound field, the observer acquires two sets of data:

[1] Care needs to be taken on defining losses: If a bubble is very much greater than resonance size, its pulsation amplitude is small, but the scattering losses can be large simply because of its size compared to the acoustic wavelength.

(I) the time history of the driving sound field; and

(II) the time history of the bubble volume.

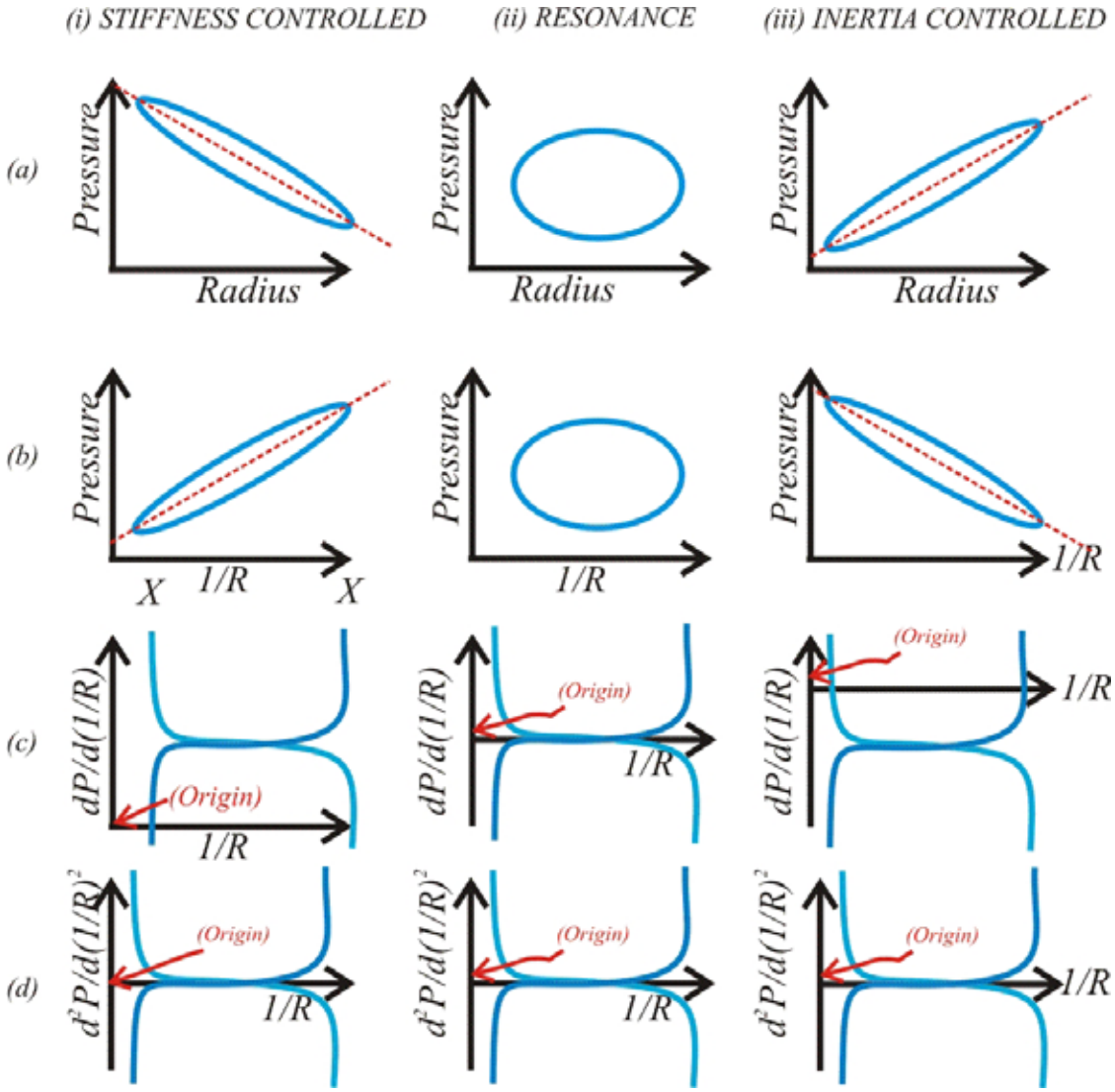

Figure 1. Schematic of the plots that could be obtained from the steady-state maps generated if the bubble size is determined simultaneously with the amplitude and phase of the insonifying field. See text for details (including discussion of how this scheme could fail because of the influence of dynamic terms).

The problems is to use these to find various unknowns, including the polytropic index (κ), the surface tension (σ) and the dissipation. The following subsections explore how this problem may be approached. The dynamic problem is examined in Section 2.2, the analysis being extended to the linear terms in the steady state only. This analysis shows the difficulties associated in separating out the polytropic index (κ)

from the surface tension (σ), since both appear together in linked form through the expression for the gas pressure within the bubble. Whilst this analysis can be used to obtain estimations, therefore, it is useful first to explore the quasi-static limit, as is done in Section 2.2. This regime is important because, if the bubble pulsations are such that the dynamical terms of negligible, the quasi-static limit allows the effects of the polytropic index (κ) from the surface tension (σ) to manifest themselves in separate variables, which are amenable to direct observation. These can then be translated to values appropriate for other insonification conditions.

2.1 The quasi-static lossless limit

Assume for the moment that the bubble dynamics occur over timescales that allow quasi-static approximations to be used. In practice this means that the sound field drives the bubbles at much less than the pulsation resonance frequency of the bubble. Furthermore assume that there is no dissipation. In this limit, the pressure in the liquid at the bubble wall (p_{L}) equals the sum of the static pressure in the liquid (p_0) and the applied pressure field ($P(t)$) which, when the Laplace pressure ($p_\sigma = 2\sigma\left(4\pi/3V\right)^{1/3}$) is taken into account, must balance the sum of the gas (p_{g}) and vapour pressures (p_{v}) in the bubble. That is to say that the internal pressure within the bubble is p_{i} where:

$$\left.\begin{array}{l} p_{\mathrm{i}} = p_{\mathrm{g}} + p_{\mathrm{v}} = p_{\mathrm{L}} + p_\sigma \Rightarrow \\ p_{\mathrm{L}} = p_{\mathrm{g}} + p_{\mathrm{v}} - p_\sigma \end{array}\right. , \tag{1}$$

and

$$p_{\mathrm{L}} = p_0 + P(t)\,. \tag{2}$$

If the gas is ideal with pressure $p_{\mathrm{g}}(t)$ (taking value $p_{\mathrm{g,e}}$ when $V = V_0$), then $p_{\mathrm{g}}V^\kappa = p_{\mathrm{g,e}}V_0^\kappa$. An equation of dynamics in terms of bubble volume is useful [2,46-48] as certain terms (such as the gas pressure) can be expressed in terms of volume even if the bubble loses sphericity. Whilst the technique can readily be cast in terms of the bubble volume, for convenience the following analysis with use the bubble

radius as this is the more usual output from photographic data (and the calculation of volumes from this can introduce some numerical errors [2]). The approach can readily be adapted for bubbles with shell properties. From (1) and (2):

$$P(t) = p_g + p_v - p_0 - p_\sigma = p_{g,e} R_0^{3\kappa} (R^{-1})^{3\kappa} + p_v - p_0 - 2\sigma / R \qquad (3)$$
$$\Rightarrow \frac{\partial P}{\partial (R^{-1})} = 3\kappa p_{g,e} R_0^{3\kappa} (R^{-1})^{3\kappa-1} + 2\sigma = \xi (R^{-1})^{3\kappa-1} + 2\sigma \quad ,$$

assuming that the surface tension is not a function of the bubble radius $R(t)$ (if it were to be, this approach could readily be adapted). At first sight it would seem from equation (3) that a plot of $\partial P / \partial (R^{-1})$ against $R^{1-3\kappa}$ would, in this quasi-static limit, yield the surface tension σ through the intercept regardless of the value of κ, which is yet to be determined. Therefore several curves could be plotted for a number of putative values of κ, and all these curves should extrapolate back to a common intercept at 2σ. Each curve would have a gradient of $\xi = 3\kappa p_{g,e} R_0^{3\kappa}$, and given that a putative value of κ was used to derive each, these gradients provide an estimate for $p_{g,e} R_0^3$.

There are however some complexities associated with this simple scheme. In the absence of dissipation in steady state, the values of *P* and *R* map one-to-one, and the locus of points in the *PV* plane is a single line (which has constant gradient if the bubble dynamics are linear, and a changing gradient if not) [28,41-44]. With dissipation, a loop of finite area is mapped out and the value of κ changes during the cycle. At least twice in each cycle (more in some circumstances, e.g. during two-frequency insonification), the value of $\partial P / \partial (R^{-1})$ must become zero, and also become so large as to undefined. This is demonstrated in Figure 1(c). By plotting the pressure against the reciprocal of the bubble radius (Figure 1(b), it is simple to sketch out the expected form of the plot of a plot of $\partial P / \partial (R^{-1})$ against R^{-1} (Figure 1(c)). There are clearly features associated with the turning points of the loop (when the bubble achieves maximum and minimum size), and whilst they contain valuable information, for the purposes of this preliminary analysis the gradients and intercepts are more easily interpreted (in terms of ((3))) away from these points (in the same way

as the spine of the *PV* loop can be used to determine the sound speed both during linear (when the spine is straight) and nonlinear (when the spine is curved) [41,42]. The spines of loops are shown as the red dashed lines in Figures 1(a) and (b). The formulation of equations (1)-(3) can be interpreted simply in the absence of dissipation, since there is only a single value of $\partial P/\partial(R^{-1})$ during the oscillation. Recalling that, furthermore, the physics in this subsection assumes quasi-static conditions. Both the conditions for low dissipation and quasi-static conditions tend to be better met when the bubble is driven at very low frequencies (which would produce plots like Figure 1(a)). However at higher frequencies, and where the dissipation is greater, the bubble dynamics do not conform with these conditions.

The same issues become compounded differentiating of (3) with respect to R^{-1} (a more detailed approach need not rely on the assumption that the variation of σ with volume is negligible):

$$\frac{\partial^2 P}{\partial(R^{-1})^2} = 3\kappa(3\kappa-1)p_{\mathrm{g,e}}R_0^{3\kappa}(R^{-1})^{3\kappa-2} = 3\kappa(3\kappa-1)p_{\mathrm{g,e}}R_0^2\left(\frac{R^{-1}}{R_0^{-1}}\right)^{3\kappa-2} \tag{4}$$

and therefore

$$\ln\frac{\partial^2 P}{\partial(R^{-1})^2} = (3\kappa-2)\ln(R^{-1}) + 3\kappa(3\kappa-1)p_{\mathrm{g,e}}R_0^{3\kappa} \tag{5}$$

and

$$\ln\frac{\partial^2 P}{\partial(R^{-1})^2} = (3\kappa-2)\ln\left(\frac{R^{-1}}{R_0^{-1}}\right) + 3\kappa(3\kappa-1)p_{\mathrm{g,e}}R_0^2 \tag{6}$$

Simple examination of the equation suggests some useful trends, although (as with use of equation (3)) the physics of the situation may make these routes difficult to implement. If $\partial^2 P/\partial(R^{-1})^2$ were to be greater than zero at all times, then plotting $\ln(\partial^2 P/\partial(R^{-1})^2)$ against $\ln(R^{-1})$ would from (3) yield an estimate of κ through the gradient. In principle this could then be used to find the product $p_{\mathrm{g,e}}R_0^{3\kappa}$ from the intercept, although in practice this might entail considerable extrapolation. Therefore if a sufficiently robust estimate for R_0 is known (e.g. from the bubble size before the

onset of insonification) then plotting $\ln(\partial^2 P/\partial(R^{-1})^2)$ against $\ln(R^{-1}/R_0^{-1})$ might be thought of as providing an estimate of the gradient of $(3\kappa-2)$ and thereby make available a better-defined intercept of $3\kappa(3\kappa-1)p_{g,e}R_0^2$, from which the gas pressure at equilibrium can be obtained ($p_{g,e}$).

However this simple scheme is not so easy to implement. Dissipation will generate negative values of $\partial^2 P/\partial(R^{-1})^2$ because of the influence of the turning points of the loop (Figure 1(d)), such that a simple interpretation of (5) (or (6) if R_0 has been estimated with sufficient accuracy from the pre-insonification conditions or from (3)) to determine an estimate of κ must be applied to data away from these points.

Most importantly, the fundamental equations on which this analysis is based pertain to static conditions. As such, the scheme presented in this section might be expected to work at very low frequencies of insonification, but to become inaccurate when dynamical terms (e.g. those related to the bubble wall speed or acceleration) become large, as would occur for example at resonance. Therefore whilst the scheme shown in Figure 1(i) might work, that shown in Figure 1(ii) would be inaccurate.

Because of this, the following section investigates how the dynamical terms can enter into the analysis.

2.2 The dynamic small-amplitude steady-state regime

Incorporation of only viscous losses into the nonlinear equation of dynamics for the bubble produces the well-known Rayleigh-Plesset equation 'in the radius frame' [2]:

$$R\ddot{R}+\frac{3\dot{R}^2}{2}=\frac{1}{\rho_0}\left(\left(p_0+\frac{2\sigma}{R_0}-p_v\right)\left(\frac{R_0}{R}\right)^{3\kappa}+p_v-\frac{2\sigma}{R}-\frac{4\eta\dot{R}}{R}-p_0-P(t)\right). \tag{7}$$

where R_0 is the unperturbed bubble radius, where ρ_0 is the unperturbed liquid density, η is the shear viscosity of the liquid, and p_∞ is the liquid pressure far from

the bubble, which is here assumed to consist of a static pressure p_0 and an applied acoustic field $P(t)$, such that $p_\infty = p_0 + P(t)$. As in section 3.1, a polytropic gas law has been used to evaluate the liquid pressure at the bubble wall (p_L), and use of the polytropic index (κ) adjusts the gas stiffness for reversible heat flow across the bubble wall, but does not describe any net thermal losses. The only dissipation present in (7) occurs through viscous losses.

This study will now consider the effect of taking a small-amplitude linearised expansion of (7). This Appendix gives an alternative linear expansion for the Rayleigh-Plesset equation (7) in the steady state linear regime to that shown in section 3.2, by defining the driving force as

$$P(t) = A\cos\omega t\,, \tag{8}$$

and then seeking the bubble response:

$$R(t) = R_0 + B\cos\omega t + C\sin\omega t = R_0 + \sqrt{B^2 + C^2}\,\cos(\omega t + \Theta)\,. \tag{9}$$

Differentiation of (9) with respect to time gives:

$$\dot{R}(t) = -B\omega\sin\omega t + C\omega\cos\omega t\,, \tag{10}$$
$$\ddot{R}(t) = -B\omega^2\cos\omega t - C\omega^2\sin\omega t\,.$$

Substitution of these into (7) gives:

$$
\begin{aligned}
&-\left(R_0 + B\cos\omega t + C\sin\omega t\right)\left(B\omega^2\cos\omega t + C\omega^2\sin\omega t\right) \\
&+\frac{3\left(-B\omega\sin\omega t + C\omega\cos\omega t\right)^2}{2} \\
&= \frac{1}{\rho_0}\begin{pmatrix}
\left(p_0 + \dfrac{2\sigma}{R_0} - p_\mathrm{v}\right)\left(1 + \dfrac{B}{R_0}\cos\omega t + \dfrac{C}{R_0}\sin\omega t\right)^{-3\kappa} + p_\mathrm{v} \\
-\dfrac{2\sigma}{R_0}\left(1 + \dfrac{B}{R_0}\cos\omega t + \dfrac{C}{R_0}\sin\omega t\right)^{-1} \\
-\dfrac{4\eta\left(-B\omega\sin\omega t + C\omega\cos\omega t\right)}{R_0}\left(1 + \dfrac{B}{R_0}\cos\omega t + \dfrac{C}{R_0}\sin\omega t\right)^{-1} \\
-p_0 - A\cos\omega t
\end{pmatrix}.
\end{aligned}
\tag{11}
$$

Expansion of this, ignoring the DC terms and terms of second order or higher, gives:

$$
\begin{aligned}
&-\left(R_0 B\omega^2\cos\omega t + R_0 C\omega^2\sin\omega t\right) = \\
&= \frac{1}{\rho_0}\begin{pmatrix}
\left(p_0 + \dfrac{2\sigma}{R_0} - p_\mathrm{v}\right)\left(1 - \dfrac{3\kappa B}{R_0}\cos\omega t - \dfrac{3\kappa C}{R_0}\sin\omega t\right) + p_\mathrm{v} \\
-\dfrac{2\sigma}{R_0}\left(1 - \dfrac{B}{R_0}\cos\omega t - \dfrac{C}{R_0}\sin\omega t\right) \\
-\dfrac{4\eta\left(-B\omega\sin\omega t + C\omega\cos\omega t\right)}{R_0} - p_0 - A\cos\omega t
\end{pmatrix}.
\end{aligned}
\tag{12}
$$

which further simplifies as follows:

$$
\begin{aligned}
&-\left(R_0 B\omega^2\cos\omega t + R_0 C\omega^2\sin\omega t\right) = \\
&= \frac{1}{\rho_0}\begin{pmatrix}
\left(p_0 + \dfrac{2\sigma}{R_0} - p_\mathrm{v}\right)\left(-\dfrac{3\kappa B}{R_0}\cos\omega t - \dfrac{3\kappa C}{R_0}\sin\omega t\right) \\
-\dfrac{2\sigma}{R_0}\left(-\dfrac{B}{R_0}\cos\omega t - \dfrac{C}{R_0}\sin\omega t\right) \\
-\dfrac{4\eta\left(-B\omega\sin\omega t + C\omega\cos\omega t\right)}{R_0} - A\cos\omega t
\end{pmatrix}.
\end{aligned}
\tag{13}
$$

It is interesting to consider what the effect on the physics has been of the mathematical operation involved in eliminating the DC terms and the terms that are of

quadratic order or higher in the expansion which transforms (7) into (13). By undertaking this elimination, the following approximations have effectively been implemented. The term $3\dot{R}^2/2$ from (7) has made no finite contribution. The term $R\ddot{R}$ has been replaced by $R_0\ddot{R}$. The term $4\eta\dot{R}/R$ has been replaced by $4\eta\dot{R}/R_0$.

The unknowns B and C can now be determined from (13). Equating the cosine terms on both side of (13) gives:

$$-R_0B\omega^2=\frac{1}{\rho_0}\left(\left(p_0+\frac{2\sigma}{R_0}-p_v\right)\left(-\frac{3\kappa B}{R_0}\right)+\frac{2\sigma B}{R_0^2}-\frac{4\eta C\omega}{R_0}-A\right). \tag{14}$$

which can be rewritten as

$$a_2B+a_1C=\frac{A}{\rho_0} \tag{15}$$

$$a_1=-\frac{4\eta\omega}{\rho_0R_0}$$

$$a_2=R_0\omega^2+\frac{2\sigma}{\rho_0R_0^2}-\left(p_0+\frac{2\sigma}{R_0}-p_v\right)\left(\frac{3\kappa}{\rho_0R_0}\right)$$

It is important to note that reflects the viscous losses, and is a combined term incorporating σ and κ which reflects the pressure within the bubble gas and the pulsation resonance frequency. Equating the sine terms on both side of (13) gives:

$$-R_0C\omega^2=\frac{1}{\rho_0}\left(\left(p_0+\frac{2\sigma}{R_0}-p_v\right)\left(-\frac{3\kappa C}{R_0}\right)+\frac{2\sigma C}{R_0^2}+\frac{4\eta B\omega}{R_0}\right). \tag{16}$$

From (16)

$$\frac{B}{C}=-\frac{\rho_0R_0}{4\eta\omega}\left(R_0\omega^2+\frac{2\sigma}{\rho_0R_0^2}-\left(p_0+\frac{2\sigma}{R_0}-p_v\right)\left(\frac{3\kappa}{\rho_0R_0}\right)\right)=\frac{a_2}{a_1}. \tag{17}$$

Substitution of (17) into (15) gives:

$$B = \frac{a_2 A}{\rho_0 (a_2^2 + a_1^2)}. \tag{18}$$

and

$$C = \frac{a_1 A}{\rho_0 (a_2^2 + a_1^2)}. \tag{19}$$

The amplitude of the bubble wall pulsation is

$$\sqrt{B^2 + C^2} = \frac{A}{\rho_0 \sqrt{a_2^2 + a_1^2}} \tag{20}$$

$$= \frac{A}{\rho_0 \sqrt{\left(R_0\omega^2 + \frac{2\sigma}{\rho_0 R_0^2} - \left(p_0 + \frac{2\sigma}{R_0} - p_v \right)\left(\frac{3\kappa}{\rho_0 R_0} \right) \right)^2 + \left(\frac{4\eta\omega}{\rho_0 R_0} \right)^2}}$$

and the phase relationship from (9) is:

$$\tan\Theta = -C/B = -\frac{a_1}{a_2} = \frac{4\eta\omega}{\left(R_0^2\omega^2\rho_0 + \frac{2\sigma}{R_0} - 3\kappa\left(p_0 + \frac{2\sigma}{R_0} - p_v \right) \right)} \tag{21}$$

This expression is sensible, as it agrees with the physics reasoned out in Figure 2.

Consider when $\omega \to 0$, the quasi-static condition which corresponds to the very low-frequency limit of the stiffness-controlled regime, when the insonification frequency is much less than the bubbles resonance (i.e. $\omega \to 0; \omega << \omega_0$, where ω_0 is defined below in equation (22)). Here, if the driving pressure is a cosine wave (equation (8) and Figure 2(b)), then because the bubble will be contracting during the compressive half-cycle and expanding during the rarefaction half-cycle of the driving pressure field, then the phase angle Θ in equation (9) will be such that $\Theta \to \pi$. As a result,

$\tan\Theta \to 0$ as shown in Figure 2(b). This is the outcome predicted by equation (21), which is the very low frequency limit tends to, i.e. $\tan\Theta = 4\eta\omega/((2\sigma/R_0) - 3\kappa(p_0 + (2\sigma/R_0) - p_v)) \to 0$ when $(\omega \to 0; \omega << \omega_0)$.

Similarly when $\omega \to \infty$, at the high frequency limit of the inertia-controlled regime, then the bubble will be expanding during the compressive half-cycle, and contracting during the rarefaction half-cycle, of the driving pulse. This condition is shown in Figure 2(d), to which equation (9) complies if $\Theta \to 0$. This would mean that $\tan\Theta \to 0$, and this result is predicted by equation (21), which is this very high frequency limit tends to $\tan\Theta = 4\eta/(R_0^2\omega\rho_0) \to 0$ when $(\omega \to \infty; \omega >> \omega_0)$.

When the driving frequency is small but finite, then the oscillation is as given by the dashed purple line in Figure 2(b). This corresponds to the phase factor Θ in equation (9) being slightly less than π. This would produce a value of $\tan\Theta$ which is small and negative (Figure 2(d)). This is the outcome predicted by equation (21), which is the very low frequency limit tends to $\tan\Theta = 4\eta\omega/((2\sigma/R_0) - 3\kappa(p_0 + (2\sigma/R_0) - p_v)) = -4\eta\omega/(3\kappa(p_0 - p_v) + (3\kappa - 1)(2\sigma/R_0))$ which is small and negative (since the smallest value which κ can take is unity, corresponding to isothermal conditions).

Consider when $\tan\Theta$ becomes undefined. This occurs when the denominator of (21) becomes zero, i.e. when $\omega = \omega_0$, where

$$\omega_0 = \frac{1}{R_0}\sqrt{\left(p_0 + \frac{2\sigma}{R_0} - p_v\right)\frac{3\kappa}{\rho_0} + \frac{2\sigma}{\rho_0 R_0}} \tag{22}$$

and shows the condition of resonance, as expected. This allows (21) to be rewritten as follows:

$$\tan\Theta = \frac{4\eta\omega}{\rho_0 R_0^2\left(\omega^2 - \omega_0^2\right)} \tag{23}$$

which indicates that $\tan\Theta<0$ for $0<\omega<\omega_0$ (i.e. in the stiffness-controlled regime), and $\tan\Theta>0$ in the inertia-controlled regime, in agreement with the physics-based reasoning used to derive Figure 2. Furthermore, it shows that, at resonance, $\tan\Theta$ is undefined, which occurs for the condition $\Theta=\pi/2$ (Figure 2(c)).

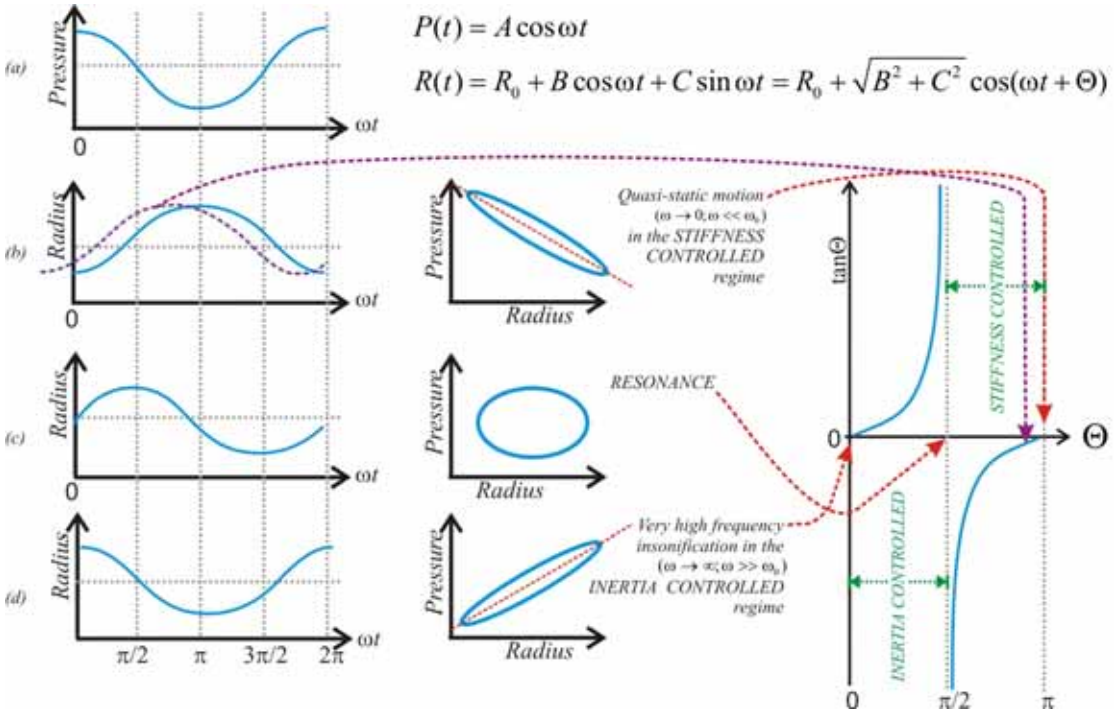

Figure 2. Schematic of the bubbles response in the linear steady state for insonification by a pressure field of the form $P(t)=A\cos\omega t$. See text for details.

The question remains as to how this phase can be used to determine bubble parameters. Key to the method is measurement of the phase of the bubble oscillation with respect to the phase of the driving field, just as was introduced for the quasi-static case described in Section 2.1.

Assume that plots of the bubble radius or volume have been obtained, and plotted against the pressure (with the phase relation known), to form plots of the form shown in Figure 1(a). The data for these could come from simulation or from high speed photography (section 1), Mie scattering [37-39], or envelope modulation of a high

frequency ultrasonic beam [40] etc. The value of $\tan\Theta$ is readily obtained from the gradient of the spine of the plots in Figure 1(a) and (b).

If the phase of the oscillation is monitored, this gives a far more precise way of measuring the position of the resonance, since the phase changes so dramatically about the resonance. Simple measurement of the resonance frequency on its own, however, does not allows identification of σ and κ, since both appear as unknowns in equation (22). Use can of course be made of the relative sizes of their respective terms within the square root of (22), the surface tension term generally being smaller for macroscopic bubbles. However all this does is make the resonance frequency insensitive to σ, such that it cannot be determined from (22) if this approximation is made. Therefore alternative information must be used, as will now be discussed.

Having used the phase to identify the resonance, the amplitude at resonance from (20) can be measured, and compared to the predicted amplitude:

$$\sqrt{B^2 + C^2} = \frac{A}{\rho_0 \sqrt{a_2^2 + a_1^2}} \tag{24}$$

$$= \frac{A}{\rho_0 \sqrt{\left(R_0\omega_0^2 + \frac{2\sigma}{\rho_0 R_0^2} - \left(p_0 + \frac{2\sigma}{R_0} - p_v \right)\left(\frac{3\kappa}{\rho_0 R_0} \right) \right)^2 + \left(\frac{4\eta\omega_0}{\rho_0 R_0} \right)^2}}$$

Here again however it is not possible to uniquely identify σ and κ and η, although again use can be made of the relative size of the additive terms within the square root.

There are therefore three unknowns, with only two equations. If however the rate of change of the phase with respect to the insonification frequency is monitored as the frequency varies, the damping is immediately apparent, a fundamental outcome of the physics of a damped linear system. It might therefore be assumed that inversion of (23) can be applied right across the range of insonification, from very high to very low frequencies, to determine the shear viscosity, with particularly sensitivity at resonance. Such an approach, however, needs to be treated with caution, because although the only source of dissipation in (7) is through viscous losses, in practice

there are other sources of loss when a bubble pulsates (associated with acoustic radiation losses, thermal losses, and wall effects). Hence the inversion of (23) will generate the effective shear viscosity, the value of η which is augmented to account for these other sources of loss as best it can (given that these other sources of loss might not readily be described in (7) by a term of the form $4\eta\dot{R}/R$ [2]). Such an effective viscosity is by no means without value. Furthermore, the importance of the various damping mechanisms can be determined by adding and subtracting the various mechanisms, as included in more sophisticated formulations than that used in Section 2.2 [42], and noting the effect on the *PVt* plot, and comparing this to the effective viscosity. Recall that the spine of the plot reflects the stiffness (Figure 1).

If the measured phase response across a wide frequency range is to be exploited, a simple way would be to use the measured value for ω_0 in (23). However the variation of $\tan\Theta$ with frequency across a wide frequency range can be used to obtain estimates of σ and κ, since

$$\frac{1}{\tan\Theta} = \frac{R_0^2\omega\rho_0 + \dfrac{2\sigma}{\omega R_0} - \dfrac{3\kappa}{\omega}\left(p_0 + \dfrac{2\sigma}{R_0} - p_v\right)}{4\eta} \tag{25}$$

Combining the measured amplitude and the measured phase as the frequency varies across a range provide another method of estimating this effective viscosity, and the combined term incorporating σ and κ which reflects the pressure within the bubble gas:

$$\begin{aligned}\sqrt{B^2+C^2} &= \frac{A}{\rho_0\sqrt{a_2^2+a_1^2}} = \frac{A}{a_2\rho_0\sqrt{1+a_1^2/a_2^2}} \\ &= \frac{A}{\rho_0\left(R_0\omega^2 + \dfrac{2\sigma}{\rho_0 R_0^2} - \left(p_0 + \dfrac{2\sigma}{R_0} - p_v\right)\left(\dfrac{3\kappa}{\rho_0 R_0}\right)\right)\sqrt{1+\left(\tan\Theta\right)^2}} \\ &= \frac{A}{a_1\rho_0\sqrt{1+a_2^2/a_1^2}} = \frac{-AR_0}{4\eta\omega\sqrt{1+\left(\dfrac{1}{\tan\Theta}\right)^2}}\end{aligned} \tag{26}$$

Of course, if the amplitude of oscillation is sufficiently great, which is of particular interest around the resonance, then a higher order expansion will allow exploitation of the nonlinear variation of the relevant parameters with the driving amplitude *A*.

Whilst σ and κ are still coupled in equations (23)-(26), they provide a route for the experimentalist to exploit these relationships through appropriare choice of experimental conditions. Options include the choice of quasi-static conditions (Section 2.1), or undertaking repeated experiments as p_0 is varied, in order to identify σ and κ separately.

3 Conclusions

An increasing number of laboratories have access to high speed cameras for studying the dynamics of ultrasonic contrast agents, single-bubble sonoluminescence etc.. Mie scattering and other techniques have been available for many years. Provided the sound field is recorded and synchronised with the movie, such studies provide measurements of three dynamic parameters: time, bubble volume, and the driving sound field. Study of the evolution of this data in *PVt* space allows direct determination of key bubble parameters, including the polytropic index, the surface tension, dissipation, gas stiffness, and the equilibrium conditions. A steady-state linear analysis was used to show the extent to which the measured phase angle between the driving field and the bubble response might be used to estimate the unknown parameter values, and the limitations imposed upon this by the coupling of the polytropic index and the surface tension in the expression for the pressure in the bubble gas (Section 2.2). To circumvent this restriction, if the bubble motion can be measured in conditions where the dynamic terms are negligible, the polytropic inde and surface tension may individually be measurable (Section 2.1).

These techniques require measurement of the pulsation and its phase relation to the driving field, which is not a simple undertaking if the bubble distorts from spherical to such an extent that it becomes difficult to identify the bubble pulsation. The Appendix

showed how, in such circumstances, the shape oscillations themselves may be used to determine the effective surface tension (which may well differ from the results of Langmuir trough measurement).

To illustrate these principles the analyses are presented for free microbubbles, but the principles can be extended to account for the presence of a shell. Such an approach offers a complementary route to fitting models which contain several unknowns, or to inversions where the accuracy of the result is not quantified by the process which finds it.

4 Appendix: How to find surface tension on a real bubble wall if the volume displacements are masked by shape oscillations

The main body of this preliminary investigation outlined an approach which might provide a complementary route to curve-fitting and, if curve-fitting is to be used, gives equations with less inherent uncertainty than the equations of motion usually used. The price for this is the restriction that the data be taken in regimes where the approximations used in those equations are relevant (e.g. small amplitude linear s steady state pulsations of Section 2.2; and, in Section 2.1, quasi-static oscillations). Furthermore, it is important to recognise that the presence of finite damping and resonances can make some datapoints poorly defined through parts of the oscillatory cycle, so that uncritical calculations based on the whole dataset would be unwise.

Key to the approach outlined in Section 2 is the measurement of bubble volume, since many of the expressions of radius in the above enter the physics through the bubble volume. If however the departure from sphericity is so great as to make such determinations difficult from high speed photography, then there are alternative techniques. One of these is the topic of this Appendix.

Whilst the pulsation mode (the spherical harmonic perturbations of order n=0) is by far the most effective contributor to the far field acoustic field radiated by a bubble, the shape oscillations give the greater visual effect, if they are present [49-51]. However whilst the n=0 pulsations is always present if there is a driving field, the higher orders corresponding to the shape oscillations ($n \geq 2$) require threshold pressures to be exceeded, and the insonification frequency to be within a given band, for a bubble of known characteristics (e.g. R_0, σ and the liquid density ρ_0) to undergo a given shape oscillation. If the applied pressure exceeds the threshold of many modes, these can all contribute to the surface oscillation, although the initial conditions (i.e. an initial distortion by tweezers or a wall) may promote one mode. The Faraday wave corresponds to that mode which has the lowest threshold pressure

(the frequency of which is close to half that of the bubble pulsation resonance frequency), and if the excitation field exceeds that threshold but not that of any other mode, then only the Faraday wave and the pulsation motion will occur on the bubble. When the bubble is driven exactly at the pulsation resonance frequency, there are two shape oscillation modes (with consecutive integer values of n) which could generate the Faraday wave, and which mode is chosen depends on whether the frequency is increasing the decreasing [52]. In order to be excited, each mode has its own threshold amplitude of spherical wall motion [53], C_T, given in the small amplitude linear limit by:

$$C_T = \sqrt{\frac{(a_n - 1)^2 + 4p}{\left(2p - 3a_n/2 + 2(n + 1/2)\right)^2 + q^2}} \tag{A1}$$

where

$$a_n = \frac{4(n-1)(n+1)(n+2)\sigma}{\rho_0 \omega^2 R_0^3}, \; p = \left(\frac{2(n+2)(2n+1)\eta}{\rho_0 \omega R_0^2} \right)^2, \; q = \frac{6(n+2)\eta}{\rho_0 \omega R_0^2} \tag{A2}$$

and the mode natural frequency is:

$$\omega_n = \sqrt{\frac{(n-1)(n+1)(n+2)\sigma}{\rho_0 R_0^3}} \tag{A3}$$

Clearly, if the other parameters in (A3) are known, the surface tension on the bubble wall can be determined from the observed mode natural frequency; and the natural frequency of several modes can be used to reduce uncertainties in those other parameters. In practice, the presence of a higher order mode could make the amplitude of the amplitude of the pulsation mode at the threshold difficult to measure (although not impossible, for example through analysis of the appropriate spectral components from Mie or ultrasonic scatter), in which case this could be calculated through application of a simple linear analysis of the form shown in section 2.2 with the drive amplitude known.

The presence of a threshold pressure for the excitation of a mode provides a powerful measurement technique, given the high sensitivities associated with threshold. Whilst this paper is primarily aimed at high speed photographic observations, Birkin, Leighton and their students did not have access to such a camera, and used an electrochemical technique to exploit this threshold in making sensitive measurements of surface tension (as well as for bubble growth and dissolution, rectified diffusion etc. [54]). In this experiment an air bubble ($R_0 \sim 2$ mm) was held under a glass rod (although later experiments used rising bubbles [28]) in an aqueous solution containing 5 mmol dm^{-3} potassium ferricyanide ($K_3[Fe(CN)_6]$ 99.5% A.C.S. Reagent, Sigma) in 0.2 mol dm^{-3} strontium nitrate ($Sr(NO_3)_2$ 99% A.C.S. Reagent, Aldrich). A 25 μm diameter Pt microelectrode was held horizontally and level with the bubble centre. In the absence of a sound field, the current resulting from reduction of the ferricyanide ($Fe(CN)_6^{3-} + e^- \rightarrow Fe(CN)_6^{4-}$) at the electrode tip is diffusion-limited, since a depletion layer builds up around the tip. If the bubble wall pulsates, convection at that frequency introduces a current enhancement at the same frequency. The onset of the Faraday wave is detected by a subharmonic component in the current. In this way, the threshold driving pressure required to excite Faraday waves as a function of the frequency of the applied acoustic wave could be plotted (Figure 3). This allows the effective surface tension on the bubble wall to be measured when known amounts of surfactant are added (unwanted surfactants were excluded through use of rigorously clean conditions). The results of Figure 3 can readily be compared with a suitable model to relate the bubble radius displacement to the applied pressure, so that equations (A1)-(A3) can be used to find the *in situ* surface tension on the bubble wall. Measurement of the ring-up time of shape modes would provide an alternative route [55].

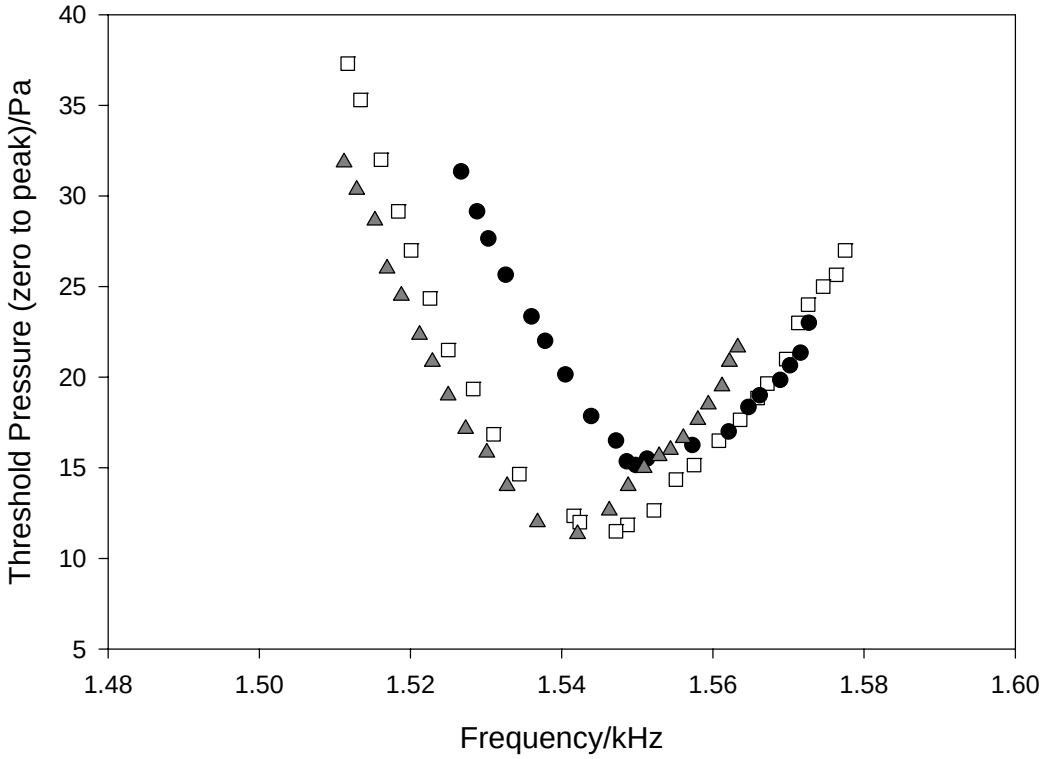

Figure 3. The frequency dependence of the threshold pressure required to generate subharmonic in the electrochemical signal, measured on a single air bubble ($R_0 \sim 2$ mm) in an electrolyte which had surface tensions, as measured by a DuNouy tensiometer, of 33.5 (□), 48.5 (▲) and 68 (•) mN/m adjusted by the addition of Triton X-100. Data from P. R. Birkin, Y. E. Watson and T. G. Leighton.

References

1 **Leighton T G, Finfer D C** and **White P R**, The problems with acoustics on a small planet. Icarus 2007 (in press).

2 **Leighton T G**, The Rayleigh-Plesset equation in terms of volume with explicit shear losses. *Ultrasonics* 2007 (in press).

3 **Palanchon P, Tortoli P, Bouakaz A, Versluis M** and **de Jong N**, Optical observations of acoustical radiation force effects on individual air bubbles. *IEEE Transactions on Ultrasonics, Ferroelectrics and Frequency Control*, **52**(1), 2005, 104- 110.

4 **Postema M, van Wamel A, ten Cate F J** and **de Jong N**, High-speed photography during ultrasound illustrates potential therapeutic applications of microbubbles. *Medical Physics*, **32**(12), 2005, 3707-3711

5 **Morgan K E, Klibanov A L, Brandenburger G H, Ferrara K W** and **Dayton P A**, Optical and acoustical observations of the effects of ultrasound on contrast agents. *IEEE Trans. Ultrason. Ferroelect. Freq. Contr*., **46**(1), 1999,220–232.

6 **de Jong N, Frinking P J A, Bouakaz A, Goorden M, Schourmans T, Jingping X** and **Mastik F.** Optical imaging of contrast agent microbubbles in an ultrasound field with a 100-MHz camera. *Ultrasound in Medicine and Biology*, **26**(3), 2000, 487–492.

7 **Chin C T, Lancée C, Borsboom J, Mastik F, Frijlink M, de Jong N, Versluis M** and **Lohse D,** Brandaris 128: a digital 25 million frames per second camera with 128 highly sensitive frames. *Rev. Sci. Instrum*. **74**, 2003, 5026–5034.

8 **Lü B L, Li Y Q, Ni H** and **Wang Y Z**, Laser-induced hybrid trap for micro-bubbles. *Applied Physics B: Lasers and Optics*, **71**(6), 2000, 801-805.

9 **Postema M, Marmottant P, Lancée C, Hilgenfeldt S,** and **de Jong N**, Ultrasound-induced microbubble coalescence. *Ultrasound in Medicine & Biology*, **30**(10), 2004, 1337-1344.

10 **Yamakoshi Y, Koshiba M, Ozawa Y** and **Masuda N**, Trapping of Micrometer Size Bubbles by Ultrasonic Waves. *Jpn. J. Appl. Phys.*, **40**, 2001, 1526-1527.

11 **May D J, Allen, J S** and F**errara K W**, Dynamics and fragmentation of thick-shelled microbubbles. *IEEE Transactions on Ultrasonics, Ferroelectrics and Frequency Control*, **49**(10), 2002, 1400- 1410.

12 **Overvelde M, Garbin V, Dollet B, Cojoc D, Ferrari E, De Jong N, Di Fabrizio E, Lohse D** and **Versluis M**, 3D optical micromanipulation of ultrasound contrast agents: bubble-wall and bubble-bubble interactions. *Proc. 19th Int. Congress on Acoustics*, 2007, Paper ULT-16-006

13 **Leighton T G, White P R** and **Marsden M A**, The one-dimensional bubble: An unusual oscillator, with applications to human bioeffects of underwater sound, *European Journal of Physics*, **16**, 1995, 275-281

14 **Leighton T G, White P R** and **Marsden M A**, Applications of one-dimensional bubbles to lithotripsy, and to diver response to low frequency sound, *Acta Acustica*, **3**, 1995, 517-529

15 **Leighton T G, Cox B T, Birkin P R** and **Bayliss T**, The Rayleigh-like collapse of a conical bubble: Measurements of meniscus, liquid pressure, and electrochemistry. *Proceedings of the 137th Regular Meeting of the Acoustical Society of America and the 2nd Convention of the European Acoustics Association (Forum Acusticum 99, integrating the 25th German Acoustics DAGA Conference),* March 1999, Paper 3APAB_1

16 **Leighton T G, Ho W-L** and **Flaxman R**, Sonoluminescence from the unstable collapse of a conical bubble. *Ultrasonics*, **35**, 1997, 399-405

17 **Leighton T G, Phelps A D, Cox B T** and **Ho W L**, Theory and preliminary measurements of the Rayleigh-like collapse of a conical bubble. *Acta Acustica,* **84**(6), 1998, 1014-1024

18 **Chen X M** and **Prosperetti A**, Thermal processes in the oscillation of gas bubbles in tubes*, J. Acoust. Soc. Am*. **104**, 1998, 1389–1398.

19 **Oguz H N** and **Prosperetti A**, The natural frequency of oscillation of gas bubbles in tubes, *J. Acoust. Soc. Am.* **103**, 1998, 3301–3308.

20 **Geng X, Yuan H, Oguz N** and **Prosperetti A**, The oscillations of gas bubbles in tubes: Experimental results*, J. Acoust. Soc. Am.* **106**, 1999, 674–681.

21 **Sassaroli E** and **Hynynen K**, Forced linear oscillations of microbubbles in blood capillaries. J. Acoust. Soc. Am., **115**(6), 2003, 3235-3243

22 **Sassaroli E** and **Hynynen K**, Cavitation threshold of microbubbles in gel tunnels by focused ultrasound. Ultrasound in Med, Biol., 33(10), 2007, 1651-1660

23 **Lauterborn W** and **Bolle H**, Experimental investigations of cavitation-bubble collapse in the neighbourhood of a solid boundary. *Journal of Fluid Mechanics*, **72**, 1975, 391-399.

24 **Dear J P** and **Field J E**, A study of the collapse of arrays of cavities. *Journal of Fluid Mechanics*, **190**, 1988, 409-425.

25 **Vogel A, Lauterborn W** and **Timm R**, Optical and acoustic investigations of the dynamics of laser-produced cavitation bubbles near a solid boundary. *Journal of Fluid Mechanics*, **206**, 1989 299-338.

26 **Ohl C-D, Philipp A** and **Lauterborn W**, Cavitation bubble collapse studied at 20 million frames per second. *Annalen der Physik*, **507**(1), 1995, 26-34.

27 **Leighton T G, Wilkinson M, Walton A J** and **Field J E**, Studies of non-linear bubble oscillations in a simulated acoustic field, *European Journal of Physics*, **11,** 1990, 352-358

28 **Leighton T G**, From seas to surgeries, from babbling brooks to baby scans: The acoustics of gas bubbles in liquids', *International Journal of Modern Physics B,* **18**(25), 2004, 3267-3314

29 **Leighton T G, Schneider M F** and **White P R**, Study of bubble fragmentation using optical and acoustic techniques, *Sea Surface Sound '94. Proceedings of the 3rd Meeting on Natural Physical Processes related to Sea Surface Sound*, M J Buckingham, J R Potter, eds., (World Scientific Publishing Ltd., Singapore) 1995, 414-428.

30 **Leighton T G, White P R** and **Schneider M F**, The detection and dimension of bubble entrainment and comminution, *Journal of the Acoustical Society of America*, **103**(4), 1998, 1825-1835

31 **Leighton T G, Phelps A D, Cox B T** and **Ho W L**, Theory and preliminary measurements of the Rayleigh-like collapse of a conical bubble. *Acta Acustica,* **84**(6), 1998, 1014-1024

32 **Leighton T G, Cox B T** and **Phelps A D**, The Rayleigh-like collapse of a conical bubble, *Journal of the Acoustical Society of America*, **107**(1), 2000, 130-142

33 **Leighton T G, Cox B T, Birkin P R** and **Bayliss T**, The Rayleigh-like collapse of a conical bubble: Measurements of meniscus, liquid pressure, and electrochemistry. *Proceedings of the 137th Regular Meeting of the Acoustical Society of America and the 2nd Convention of the European Acoustics Association (Forum Acusticum 99, integrating the 25th German Acoustics DAGA Conference),* March 1999, Paper 3APAB_1

34 **van der Meer S M, Dollet B, Goertz D E, de Jong N, Versluis M** and **Lohse D**, Surface modes of ultrasound contrast agent microbubbles. IEEE Ultrasonics Symposium, October 2006. 112-115.

35 **Leighton T G** and **Field J E**, Sonoluminescence from flow over a hydrofoil in a cavitation tunnel, *ISVR Technical Report No. 223, University of Southampton*, 1993

36 **Leighton T G, Farhat M, Field J E** and **Avellan F**, Cavitation luminescence from flow over a hydrofoil in a cavitation tunnel, *J. Fluid Mech*., **480**, 2003, 43-60

37 **Langley D S** and **Marston P L,** Critical-angle scattering of laser light from bubbles in water: measurements, models, and application to sizing of bubbles. *Applied Optics*, **23**(7), 1984, 1044-1054.

38 **Hansen G M**, Mie scattering as a technique for the sizing of air bubbles. *Applied Optics*, **24**(19), 1985, 3214-3220

39 **Holt R G, Crum L A**, Mie scattering used to determine spherical bubble oscillations. *Applied Optics*, **29**(28), 1990, 4182-4191.

40 **Phelps, A.D.** and **Leighton, T.G.** High-resolution bubble sizing through detection of the subharmonic response with a two frequency excitation technique, *Journal of the Acoustical Society of America*, 99, 1996, 1985-1992

41 **Leighton T G**, 'Nonlinear Bubble Dynamics And The Effects On Propagation Through Near-Surface Bubble Layers,' *High-Frequency Ocean Acoustics*, Eds. M.B. Porter, M. Siderius, and

W. Kuperman, (American Institute of Physics Melville, New York) *AIP Conference Proceedings* **728**, 180-193 (2004)

42 **Leighton T G, Meers S D** and **White P R**, Propagation through nonlinear time-dependent bubble clouds, and the estimation of bubble populations from measured acoustic characteristics. *Proceedings of the Royal Society A,* **460**(2049), 2004, 2521-2550

43 **Leighton T G** and **Dumbrell H A**. New approaches to contrast agent modelling. *Proceedings of the First Conference in Advanced Metrology for Ultrasound in Medicine*, *Journal of Physics: Conference Series* 1, 91-96 (2004)

44 **Leighton T G**. What is ultrasound? Progress in Biophysics and Molecular Biology, **93**, Issues 1-3 , 3-83 (2007)

45 **Leighton T G**, The Acoustic Bubble, Academic Press, 1994.

46 **Zabolotskaya E A** and **Soluyan SI**, Emission of harmonic and combination-frequency waves by air bubbles. *Sov. Phys. Acoust*., **18**, 1973, 396-398.

47 **Welsby V G** and **Safar M H**, Acoustic Non-Linearity Due to Micro-Bubbles in Water. *Acustica,* **22**, 1969/70, 177-182.

48 **Sutin A M, Yoon S W, Kim E J** and **Didenkulova I N**, Nonlinear acoustic method for bubble density measurements in water, *J. Acoust. Soc Am.,* **103**, (1998), 2377-2384.

49 **Trinh E H, Thiessen D B** and **Holt R G**, Driven and freely decaying nonlinear shape oscillations of drops and bubbles immersed in a liquid: experimental results. *Journal of Fluid Mechanics*, **364**, 1998, 253-272.

50 **Rath H J**, On the stability of gas bubbles oscillating non-spherically in a compressible liquid. *Journal of Engineering Mathematics*, **15**(3), 1981, 161-170.

51 **Versluis M, van der Meer, S M, Lohse D, Palanchon P, Goertz D, Chin C T** and **de Jong N,** Microbubble surface modes [ultrasound contrast agents]. *IEEE Ultrasonics Symposium*, **1**, 2004, 207-209.

52 **Birkin P R, Watson Y E, Leighton T G** and **Smith K L**, Electrochemical detection of Faraday waves on the surface of a gas bubble. *Langmuir Surfaces and Colloids*, **18**, 2002 , 2135-2140

53 **Francescutto A** and **Nabergoj R**, Pulsation amplitude threshold for surface waves on oscillating bubbles. *Acustica*, **41**, 1978, 215-220.

54 **Birkin P R, Leighton T G** and **Watson Y E.** The use of Acoustoelectrochemisty to investigate rectified diffusion. *Ultrasonics Sonochemistry*, **11** (3-4), 2004, 217-221

55 **Maksimov A O** and **Leighton T G**, Transient processes near the threshold of acoustically driven bubble shape oscillations, *Acta Acustica* **87**(3), 2001, 322-332